Systematic Interferometric Phase Biases and their Impact on Earth Surface Deformation Monitoring

Homa Ansari[a], Francesco De Zan[a], and Alessandro Parizzi[a]
[a] German Aerospace Center (DLR)-Remote Sensing Technology Institute (IMF)

Abstract

In this work we scrutinize the reliability of multilooked interferograms for deformation analysis. Designing a simple approach in the evaluation of the accuracy of the estimated deformation signals, we reveal a prominent bias in the deformation velocity maps. The bias is the result of propagation of small phase error of multilooked interferograms through the time series and can sum up to 6.5 mm/yr in case of using the error prone short temporal baseline interferograms. We further discuss the role of the phase estimation algorithms in significant reduction of the bias and put forward the idea of a unified intermediate InSAR product for achieving high-precision deformation monitoring.
Keywords: Big Data, Fading Signal, SAR Interferometry, Error Analysis, Time Series Analysis.

1 Introduction

Through extensive analysis of Sentinel-1 data, we observe a systematic, yet temporally inconsistent, error source in the multilooked interferograms which especially compromises the reliability of Interferometric Synthetic Aperture Radar (InSAR)-derived deformation velocity maps. The observed error is attributed to the systematic variation in the scattering properties of the sub resolution scatterers [1]. The phenomenon can be explained, for instance, by moisture variation, vegetation growth etc. A relevant research direction is on-going to interpret the physical source and model the interferometric phase of such systematic signals [2]. Complementary to the latter, this work sheds light on other aspects of the problem. Here we demonstrate:

- the presence of the systematic effects in interferograms;
- the propagated error to the deformation velocity maps;
- the effect of processing algorithms on mitigating the error.

In these demonstrations, we distinguish between two types of observations in InSAR: single-look versus the multilook interferometric phases. The former is for instance related to the Persistent Scatterers (PS), where the single complex valued pixels are exploited within the time series. The latter multilooked observations are the result of spatial averaging (i.e. multilooking). Spatial averaging is the cornerstone of many advanced InSAR time series analysis techniques, with [3] and [4] setting the two overarching trends in this regard. Although effective in improving the Signal to Noise Ratio (SNR) of the natural land covers, known as Distributed Scatterers (DS), multilooking changes the statistical properties of the interferograms and introduces peculiar physical signal. Therefore, a phase bias is observed between the single-look and multilooked observations. The study of the impact of this phase bias on Earth surface deformation retrieval is the focus of this paper.

For scrutinizing the presence and effect of the phase biases on deformation estimates, we resort to the comparison of the single-look and multilooked observations. In the following section, we firstly expand on our comparison approach. The result of the comparisons is provided in section 3. Our conclusions and recommendations finalize the paper.

This paper does not include our in-depth analysis for revealing the systematic phase biases of the multilooked interferograms, instead it highlights the consequence of such biases for the deformation estimation.

2 Methodology

We design an experiment to reveal the propagation of the phase bias of multilooked interferograms to the deformation estimates. As the benchmark of the experiment, we perform Persistent Scatterer Interferometry (PSI) to allow the deformation estimation based on pure single-look observations. Should inconsistent systematic effects exist within the multilooked interferograms, the deformation estimates vary depending on which interferograms are employed for their retrieval. We perform multiple processing rounds to corroborate this proposition.

In the first processing round, we exploit all possible interferograms within the time series to retrieve the deformation signal as explained in section 2.1. In the following processing rounds, we test the ingestion of different subsets of the interferograms for deformation estimation; the corresponding estimator for this processing is introduced in section 2.2.

The resulting deformation estimates from the different experiments are evaluated against the benchmark PSI result

to reveal the presence of bias in deformation, as explained in section 2.3.
This section expands on the theory of the comparison schemes, the result of the comparison is reported in section 3.

2.1 Phase linking on all interferograms

After its pioneering authors, we define phase linking as the estimator which retrieves $n-1$ consistent common-master interferograms from all possible $n(n-1)/2$ interferogram combinations within a stack of n acquisitions [5]. The estimated interferograms are the input for deformation retrieval. Here we shortly review the idea of phase linking. Without loss of generality, we concentrate on one DS region (see [4, 6] for algorithmic details of the DS region selection). The DS is comprised of an ensemble of spatially homogeneous region of p pixels in a time series of n Synthetic Aperture Radar (SAR) images, arranged in a matrix $\boldsymbol{Z} \in \mathbb{C}^{n\times p}$. Based on the central limit theorem, $\boldsymbol{Z}$ follows the zero-mean n-variate Complex Circular Gaussian (CCG) distribution [7]. Under the validity of this distribution, the sample covariance matrix, or its normalized version Sample Correlation Matrix (SCM), suffices for the full description of the DS. The SCM, hereafter denoted by $\boldsymbol{C}$, is a Hermitian matrix whose off diagonal elements pertain to all possible multilooked interferograms $\boldsymbol{I}_{ik}$ within the SAR time series and its temporal coherence $\boldsymbol{\Gamma}_{ik}$, i.e:

$$\angle \boldsymbol{C}_{ik} = \boldsymbol{I}_{ik} = \Delta\phi_{ik} \tag{1}$$
$$|\boldsymbol{C}_{ik}| = \boldsymbol{\Gamma}_{ik} \tag{2}$$

The difference in phase linking techniques may be formulated as the difference in modeling the SCM [8, 9]. In an earlier work [8], we proposed a computationally efficient approach to phase linking called Eigen-decomposition-based Maximum-likelihood-estimator of Interferometric phase (EMI). This proposal decreases the computational cost by reformulating phase estimation into the following Eigen-decomposition problem [8]:

$$\hat{\boldsymbol{\phi}} = \angle(\text{argmin}_{v_i}\{\boldsymbol{v}_i^H\ (\boldsymbol{C}\circ\boldsymbol{\Gamma}^{-1})\ \boldsymbol{v}_i\}); \tag{3}$$
$$\text{subject to} \quad \boldsymbol{v}_i^H\boldsymbol{v}_i = 1$$
$$\text{and} \quad \boldsymbol{v}_i^H\boldsymbol{v}_k = 0;$$

where $\boldsymbol{v}_i$ is an arbitrary complex vector of size $n\times 1$ and $\circ$ is the Hadamard product. Note that, as common in InSAR, the estimation of absolute phase is ambiguous. An arbitrary image in the time series is selected as the master, its phase is set to zero and the remaining phases are measured relative to this arbitrary datum. $\hat{\boldsymbol{\phi}}$ is a vector of n wrapped phase values relative to the selected master. It contains the *consistent* interferometric phase component within the exploited interferograms. This phase information is used for the retrieval of the deformation signal.

2.2 Phase linking on interferogram subsets

To allow the ingestion of different subsets of interferograms and evaluate path-dependency of the deformation estimates, we designed a variation of the Small BAseline Subset approach (SBAS) technique of [3]. The difference with respect to the conventional SBAS is two-fold:

- The baseline constrain is only imposed on the temporal separation between the acquisition pairs.
- Phase linking is performed on the chosen interferogram subset. Deformation estimation follows based on these estimated phases.

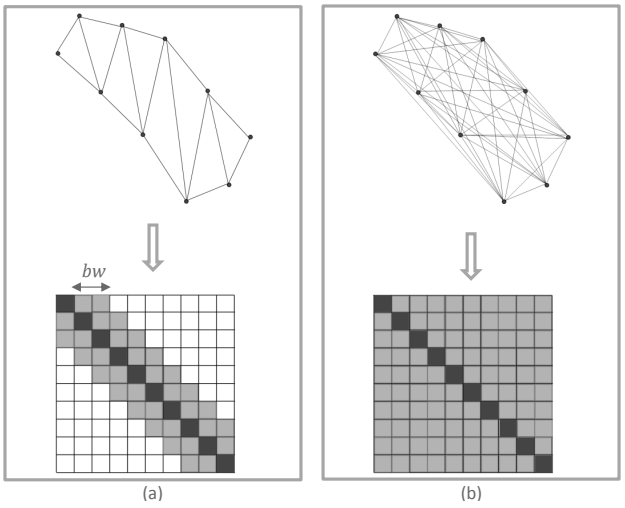

Figure 1 Different levels of data exploitation for deformation analysis. Top sketch mimics SAR images with dots and the exploited interferograms with arcs; the sketch below shows the corresponding SCM where diagonal elements refer to the images and the filled off-diagonals represent the employed interferograms. Images are assumed to be temporally sorted. (a) partial exploitation of the data with short temporal baseline interferograms of up to band bw, and (b) the full exploitation of the interferograms with full SCM.

Performing phase linking on the interferogram subsets, the designed approach is less prone to the propagation of phase unwrapping errors. Hereafter this approach is referred to as Enhanced Short temporal BAseline Subset approach (E-StBAS).
The chosen subset is comprised of bw number of shortest temporal baseline interferograms per acquisition in the time series. The total number of the employed interferograms in E-StBAS of bandwidth bw follows from:

$$m = \frac{bw}{2}(2n - bw - 1) \tag{4}$$

Compared to the conventional phase linking, here a band matrix will replace the full SCM (see Fig. 1). The bandwidth of the matrix is defined by the parameter bw. The consistent phase based on these interferograms is reconstructed following the below iterative optimization:

$$\hat{\boldsymbol{\phi}}_i^p = \angle\left(\frac{1}{bw}\sum_{k=1}^{bw}\boldsymbol{\Gamma}_{i,i+k}\exp(j\Delta\phi_{i,i+k} - j\hat{\boldsymbol{\phi}}_{i+k}^{p-1})\right) \tag{5}$$

The iterations can be initialized by the largest eigenvector of the band matrix $\boldsymbol{C}^{bw}$, i.e.:

$$\hat{\boldsymbol{\phi}}^0 = \angle(\text{argmax}_{v_i}\{\boldsymbol{v}_i^H\boldsymbol{C}^{bw}\boldsymbol{v}_i\}); \tag{6}$$
$$\text{subject to} \quad \boldsymbol{v}_i^H\boldsymbol{v}_i = 1,$$
$$\text{and} \quad \boldsymbol{v}_i^H\boldsymbol{v}_k = 0.$$

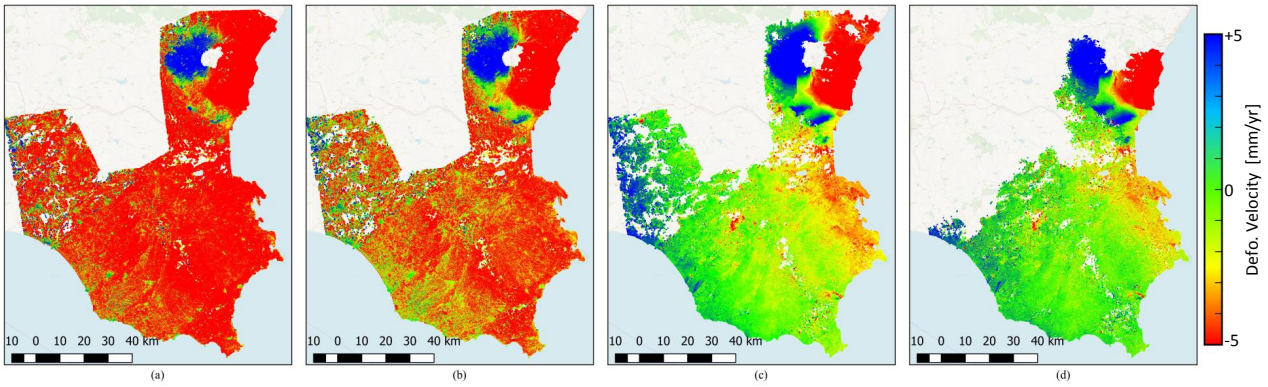

Figure 2 Deformation velocity maps retrieved by three different DS processing schemes of (a) E-StBAS5 with $bw = 5$ (b) E-StBAS10 with $bw = 10$ (c) EMI using full SCM; as compared to (d) the benchmark PSI processing. The reference point is identical in all maps.

In practice (6) provides a sufficient approximation such that the iteration by (5) is unnecessary. As in section 2.1, $\hat{\phi}$ contains the consistent interferometric phase component within the exploited subset. This phase information is used for the retrieval of the deformation signal.

2.3 Evaluation of Deformation Bias

Retrieving the consistent phase series for DS using either EMI or E-StBAS, the deformation signal is estimated following a 3D phase unwrapping and decomposition of signal to deformation and atmospheric components [10, 11, 4]. Two products may be retrieved from the deformation signal, namely the relative displacement time series of size $n-1$ per DS, and more concisely the modeled deformation velocity as a single parameter per DS.

The intention is to evaluate the accuracy of both DS-derived products. The conventional approach to validation is to use independent geodetic measurements; provided for instance by Global Navigation Satellite Systems (GNSS). However, being interested in detailed evaluation of the DS behavior over different land cover, the available sparse GNSS networks would not suffice for our analysis.

We instead opt for the PS-derived deformation signal as the benchmark for validation. Being single-look observations, the PS are exempt of phase inconsistencies. Therefore, the associated deformation shall be free of systematic biases. Furthermore, the spatial distribution of PS is by far denser than the available GNSS measurements.

The performance evaluation is conducted as following: spatial grids of size 1 km^2 is chosen for down-sampling both displacement time series and deformation velocity maps. For all PS and DS within the defined reference grid cells, a weighted average of the deformation signal substitutes the sparse estimates. The weighting is based on the a posteriori coherence of PS [11] and DS [4]. For the latter scatterers, the clutter is disregarded using a constant false alarm rate detector. Following this approach the down-sampled DS and PS deformations are directly comparable. From this point on, the calculation of the estimation bias in deformation products is straight-forward:

$$\epsilon_d(x,y) = \mathbb{E}\{d_{\mathrm{DS}}(x,y)\} - \mathbb{E}\{d_{\mathrm{PS}}(x,y)\} \qquad (7)$$

where $\mathbb{E}$ is the mentioned weighted averaging operator, x, y are the spatial coordinates of the down-sampled grid and ϵ_d is the evaluated bias. d can represent either the displacement values in the time series or the deformation velocity.

This evaluation will result in a time series of displacement biases as well as the overall deformation velocity bias for the entire time series. Both biases are calculated over the down-sampled spatial grid.

Table 1 Summary of the compared approaches for the estimation of deformation velocity. PSI is used for bias and dispersion.

Phase Estimation	SCM Bandwidth bw	No. of Ifgrms. m	Defo. Bias [mm/yr]	Defo. Variance [mm/yr]
E-StBAS5	5	905	-6.50	2.58
E-StBAS10	10	1785	-3.05	1.55
EMI	full SCM	16836	-0.24	0.70

3 Results

For the study of the biases, a test site is chosen in the island of Sicily-Italy. The test site is regularly monitored by Sentinel-1 A and B, with abundant data. The land cover is heterogeneous to observe the behavior of different DS types. The area is investigated by different studies, e.g, [12, 13], and potentially allows independent performance comparison.

The data set is comprised of 184 acquisitions from October 2014 to September 2018 of descending track. It covers approximately 15000 km^2.

Following the introduced methods in section 3, the biases in deformation velocity and displacement time series is studied in this section. Our evaluation of the phase biases in the multilooked interferograms is not provided here; however, it will be presented in the conference.

3.1 The comparison scenarios

The intention is to define a scientifically credible experiment which can isolate the impact of multilooked phases

on deformation estimation.
We perform a unified processing chain for deformation retrieval. All steps of the processing and the corresponding latent parameters are kept identical, with the exception of phase estimation. With reference to section 2, three different schemes are compared in phase estimation:

- E-StBAS with bandwidth of five;
- E-StBAS with bandwidth of ten;
- EMI performing phase linking on full SCM.

The defined experiment is summarized in table 1.
Identical to the three cases, Interferometric Wide Area Processing (IWAP) chain [14] is used for deformation estimation, with phase estimation integrated in the chain. The topographic induced phase is removed using the Shuttle Radar Topographic Mission (SRTM) Digital Elevation Model (DEM) to improve spatial stationarity in short distances. As the first step toward DS processing, the statistically homogeneous ensembles surrounding each pixel are detected. The amplitude-based Anderson-Darling statistical similarity test [6] with false alarm rate of 5% is chosen as the detection method. The search window for the test comprises of 25 and 7 looks in range and azimuth direction, respectively. The effective number of look is however approximately half in each direction. The homogeneous ensembles are exploited for adaptive multilooking of the direct interferograms as well as estimation of the SCM at DS region. A constant false alarm rate detector is further used to detect the signal bearing DS and exclude the low quality regions from the deformation analysis [16]. The latter regions pertain to fast decorrelating scatterers such as water bodies and dense vegetation.
Beside the three DS comparison cases, we perform a conventional PSI and treat the result as the benchmark for our analysis to follow. Note that in all four, the master scene and reference point are identical. Moreover, the latent latent parameters are kept identical or chosen in an data-driven fashion, to ensure the credibility of the comparisons.
Fig. 2 shows the retrieved deformation velocity map of these four described schemes. In the following sections, the results are quantitatively analyzed.

3.2 Bias in deformation velocity

We are interested in the quantitative error of the deformation velocity maps reported in Fig. 2. Following the described method in section 2.3, the PS scheme is taken as the benchmark. According to (7), the discrepancy between the velocity estimated by each three DS schemes are evaluated against this benchmark over a down-sampled grid. Fig. 3 depicts the probability density function (PDF) of the accumulated discrepancies over the entire test site. The first and second order moment of these PDFs provide a measure for the overall bias and dispersion of each method in the estimation of the deformation velocity. These performance indicators are summarized in table 1.
As revealed by the comparisons, both the bias and dispersion decrease when more interferograms are exploited for phase and consequently deformation estimation.

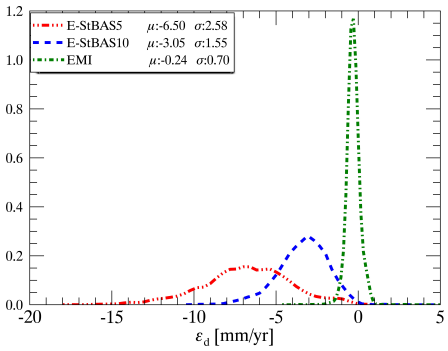

Figure 3 PDF of deformation velocity bias evaluated by (7), reported for the three DS processing schemes. The first μ and second σ order moments of these PDFs indicate the overall bias and dispersion of the velocity estimates, respectively. The increase in the number of exploited interferograms improves the overall accuracy of deformation estimation.

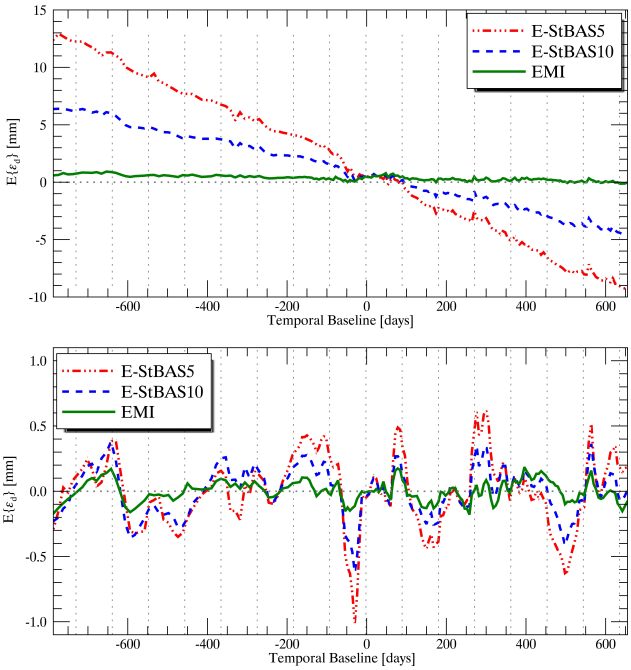

Figure 4 Temporal trends of the average bias in displacement estimation for the three compared DS schemes. top: the overall trend, bottom: the periodic behavior resulted from the removal of the linear trends. The linear variation of the displacement bias prevails the periodic changes. This implies the negligible effect of seasonal variations of the phase which may be attributed to the moisture variation.

3.3 Bias in displacements

We further extend the bias analysis to the temporal domain by evaluating the discrepancy in the displacement time series. The latter time series is the outcome of spatiotemporal phase unwrapping and the removal of topographic and atmospheric signal components. In practice the nonlinear displacements may leak to the atmospheric signal estimation and be removed from the time series, however, the issue is irrelevant to the purpose of the current study.
Similar to the previous section and following the method of section 2.3, the displacement bias between each DS scheme and the benchmark PSI result is evaluated for each single acquisition. The displacement bias is therefore eval-

uated per acquisition and over the down-sampled grid via (7).
The average displacement bias of each acquisition is provided in Fig. 4. The following are observed from this figure:

- Both the bias and dispersion of the displacement estimates increase with the temporal baseline. The error propagation is more severe where less interferograms are exploited.
- A prevailing linear trend is observed for E-StBAS5 and 10, implying the persistent presence of physical source of bias in the DS over the entire time series.
- A negligible periodic trend is observed which may be attributed to the moisture variations [1, 2].
- Using the data-adaptive solution and exploiting the full time series in EMI significantly helps in the robust estimation of displacement.

3.4 Tracking the observed bias to multilooked interferograms

In the attempt to find the source of deformation bias, we performed an in-depth analysis of the multilooked interferograms within the data stack and corroborated the presence of a systematic but inconsistent physical signal within the data stack. The magnitude of the signal decreases with temporal baseline, rendering the short temporal baseline interferograms more prone to the perturbing effects.

4 Discussion and Recommendation

From the various analysis of the previous section, the following conclusions are drawn:

- multilooked interferograms reveal a persistent systematic phase component which cannot be attributed to atmospheric or surface topography variations;
- this systematic phase component is absent in single-look phase observations;
- exploiting the temporal data redundancy in large time series renders the robustness of the phase retrieval algorithms to such phase errors;
- the major role in the gained robustness is played by the inclusion of the long temporal baseline interferograms in phase retrieval;
- phase biases are larger for shorter temporal baseline, albeit more coherent and therefore high SNR, interferograms;
- the propagation of even small phase biases in long time series compromises the accuracy of deformation velocity maps from the otherwise achievable sub-millimeter per year precision;
- the systematic phases comprise of a prominent linear and a much lower magnitude periodic signal;

The presence of phase biases have consequences for the accuracy of InSAR in deformation analysis. The problem is highly exacerbated for Big Data processing. Common practice in processing large time series is to mostly exploit the short temporal baseline interferograms; similar to the designed E-StBAS scheme. The reason is that short baseline interferograms are less affected by temporal decorrelation and believed to be more reliable for deformation estimation. However, the analysis of this paper proves that these interferograms are the most affected by the inconsistent systematic signals and most prone to propagate systematic errors through the time series.
In principle one could increase the number of interferograms to achieve a reliable deformation estimate. However, according to our experiments, the choice of optimum number of interferograms for reliable deformation estimates is test site and land cover dependent. Therefore, we advocate data-adaptive phase retrieval using all the possible interferograms, through sufficient modeling of the full SCM. According to our extensive wide area processing experience, partially reported in [17, 18], EMI provides a computationally efficient solution for phase estimation and does not pose a challenge for Big Data processing. Is a more efficient phase retrieval with minimum storage and input/output requirements desired for Big Data processing, we recommend the sequential estimator for reconstruction of consistent phase [19]. The accuracy of the sequential algorithm is studied and proven to retain the millimeter level target [17].
Our final recommendation is to introduce a new intermediate product level for InSAR, namely the reconstructed consistent interferometric phase series. The envisioned product would:

- contain the time-consistent physical signals such as, but not limited to, atmospheric variations and surface displacements;
- significantly reduce the interferometric phase bias and variance;
- reduce the amount of interferometric data from the original pairwise interferograms within the data stack to a time series of higher quality and, optionally, down-sampled interferograms;
- provide a unified product for deformation monitoring;
- enhance the reliability of InSAR for displacement analysis specifically for the retrieval of deformation velocity maps.

5 Literature

[1] F. De Zan, M. Zonno, and P. Lopez-Dekker, "Phase Inconsistencies and Multiple Scattering in SAR Interferometry," *IEEE Transactions on Geoscience and Remote Sensing*, vol. 53, no. 12, pp. 6608–6616, Dec. 2015.

[2] F. De Zan and G. Gomba, "Vegetation and soil moisture inversion from SAR closure phases: First experiments and results," *Remote sensing of environment*, vol. 217, pp. 562–572, 2018.

[3] P. Berardino, G. Fornaro, R. Lanari, and E. Sansosti, "A new algorithm for surface deformation monitoring based on small baseline

differential sar interferograms," *IEEE Transactions on geoscience and remote sensing*, vol. 40, no. 11, pp. 2375–2383, 2002.

[4] A. Ferretti, A. Fumagalli, F. Novali, C. Prati, F. Rocca, and A. Rucci, "A New Algorithm for Processing Interferometric Data-Stacks: SqueeSAR," *IEEE Transactions on Geoscience and Remote Sensing*, vol. 49, no. 9, pp. 3460–3470, Sep. 2011.

[5] A. Monti Guarnieri and S. Tebaldini, "On the Exploitation of Target Statistics for SAR Interferometry Applications," *IEEE Transactions on Geoscience and Remote Sensing*, vol. 46, no. 11, pp. 3436–3443, Nov. 2008.

[6] A. Parizzi and R. Brcic, "Adaptive InSAR Stack Multilooking Exploiting Amplitude Statistics: A Comparison Between Different Techniques and Practical Results," *IEEE Geoscience and Remote Sensing Letters*, vol. 8, no. 3, pp. 441–445, May 2011.

[7] R. Bamler and P. Hartl, "Synthetic aperture radar interferometry," *Inverse Problems*, vol. 14, no. 4, pp. R1–R54, Aug. 1998.

[8] H. Ansari, F. De Zan, and R. Bamler, "Efficient phase estimation for interferogram stacks," *IEEE Transactions on Geoscience and Remote Sensing*, vol. 56, no. 7, pp. 4109–4125, May 2018.

[9] H. Ansari, F. De Zan, G. Gomba, and R. Bamler, "EMI: efficient temporal phase estimation and its impact on high-precision InSAR time series analysis," in *Proc. IEEE Geoscience and Remote Sensing Symposium IGARSS*, Yokohama, Japan., 2019.

[10] A. Ferretti, C. Prati, and F. Rocca, "Permanent scatterers in SAR interferometry," *IEEE Transactions on Geoscience and Remote Sensing*, vol. 39, no. 1, pp. 8–20, Jan. 2001.

[11] B. M. Kampes, *Radar Interferometry Persistent Scatterer Technique*. Springer Netherlands, 2006.

[12] I. Zinno, M. Bonano, S. Buonanno, F. Casu, C. De Luca, R. Lanari, M. Manzo, M. Manunta, and G. Zeni, "Surface deformation mapping of italy through the P-SBAS DInSAR processing of sentinel-l data in a cloud computing environment," in *IGARSS*, IEEE. in Proc. IEEE Geoscience and Remote Sensing Symposium, 2018.

[13] M. Manunta, C. De Luca, I. Zinno, F. Casu, M. Manzo, M. Bonano, A. Fusco, A. Pepe, G. Onorato, P. Berardino *et al.*, "The parallel SBAS approach for sentinel-1 interferometric wide swath deformation time-series generation: Algorithm description and products quality assessment," *IEEE Transactions on Geoscience and Remote Sensing*, vol. 57, no. 9, pp. 6259–6281, 2019.

[14] N. Adam, F. R. Gonzalez, A. Parizzi, and R. Brcic, "Wide area Persistent Scatterer Interferometry: Current developments, algorithms and examples." IEEE, Jul. 2013, pp. 1857–1860.

[15] H. Ansari, F. Rodríguez-González, R. Brcic, and F. De Zan, "Evaluation of ensemble coherence as a measure for stochastic and systematic phase inconsistencies," in *Proc. IEEE Geoscience and Remote Sensing Symposium IGARSS*, Yokohama, Japan., 2019.

[16] H. Ansari, *Efficient High-Precision Time Series Analysis for Synthetic Aperture Radar Interferometry*. German Aerospace Center (DLR), ISSN: 1434-8454, 2019.

[17] H. Ansari, F. De Zan, and R. Bamler, "Distributed scatterer interferometry tailored to the analysis of Big InSAR Data," in *Proc. 12th European Conference on Synthetic Aperture Radar EUSAR*, Aachen, Germany., 2018.

[18] ——, "Sequential Estimator: Toward Efficient InSAR Time Series Analysis," *IEEE Transactions on Geoscience and Remote Sensing*, vol. 55, no. 10, pp. 5637–5652, Oct. 2017.